IEEE Access
Multidisciplinary | Rapid Review | Open Access Journal

Received 13 June 2023, accepted 11 July 2023, date of publication 20 July 2023, date of current version 27 July 2023.
Digital Object Identifier 10.1109/ACCESS.2023.3297147

RESEARCH ARTICLE

Traction Amplified Actuation System for Inspecting Narrow and Complex Pipes Using Enhanced Linear Antagonistic Mechanism-Bend Pipe Passage Model and Force Comparison

F. ITO[1], **(Graduate Student Member, IEEE), Y. NARUSE**[1], **K. TAKAYA**[1], **J. WATANABE**[2], **AND T. NAKAMURA**[1], **(Member, IEEE)**
[1]Faculty of Science and Engineering, Chuo University, Bunkyo, Tokyo 112-8551, Japan
[2]Pigeon Home Products Corporation, Shizuoka 417-0826, Japan
Corresponding author: F. Ito (fumio.ito.020@gmail.com)

This work was supported in part by Pigeon Home Products Corporation.

ABSTRACT This paper describes the design, experiments, and quantitative force comparison of a Pipe Inspection RObot named PI-RO II using the enhanced linear antagonistic mechanism to amplify the traction. This study aims to develop an inspection robot for long, narrow, and complex pipes requiring large traction, propulsion, and flexibility. Many types of pipe inspection robots using soft pneumatic actuators were proposed in conventional studies, focusing on compatibility, high-power characteristics, and flexibility. In a previous study, we proposed a linear antagonistic mechanism allowing the inspection robot to generate both high traction and propulsion with flexibility in narrow pipes. The large extension force of an extension actuator is distributed to the traction and propulsion. However, when large propulsion was required, traction was insufficient because the extension force of an actuator was distributed to traction and propulsion. Furthermore, the traction is decreased because the actuator's elongation/contraction length is absorbed due to the changing robot's movement path in the bending pipe. This paper described an enhanced linear antagonistic mechanism that amplified traction through the active force of multiple integrated pneumatic actuators even when large propulsion is required. Moreover, a design method is explained to keep PI-RO II's axis consistent with the center of the pipe. PI-RO II in this study inspected an upward pipeline with a length of 4.5 m, including 5 elbow pipes three times consecutively within approximately 1250 s, respectively. The function value that compares the traction and propulsion considering the effects of the applied pressure and pipe diameter required for long-distance inspection is more than 1.79 times that of the other related studies. This function value allows a comparison of the sum of traction and propulsion values of various pneumatically driven pipe inspection robots by non-dimensionalizing the inner diameter of the pipe and the pressure. This result shows PI-RO II has the possibility to generate large traction even when large propulsion is required. Therefore, we believe that the proposed mechanism will improve the moving efficiency of the pipe inspection robots.

INDEX TERMS Traction amplification method, enhancing linear antagonistic mechanism.

I. INTRODUCTION

Many long, narrow, complex pipes convey various fluent in the factory. These pipes corrode due to long-term use, decreasing transporting efficiency and fluid quality. visually inspects with the camera pushed into the pipe. However, inspecting the entire pipeline in a long, narrow pipe with multiple bends is difficult, because friction between the endoscope and the inner pipe wall prevents the transition of the operator's hand force to the endoscope tip. Therefore,

The associate editor coordinating the review of this manuscript and approving it for publication was Tao Wang.

an in-Pipe Inspection Robot is required instead of the push-in endoscope.

There are many types of in-pipe inspection robots, such as wheel-type [3], [4], [5], [6], [7], snake-type [8], [9], [10], [11], [12], cilia vibration type [13], spirochete type [14], [15], earthworm type [16], [17], [18], [19] and inchworm-type [19], [20], [21], [22], [23], [24], [25], [26], [27], [28]. Many wheel-type, snake-type in-pipe inspection robots are driven by the rotational force of an electric motor. These robots tend to be large when pulling endoscopes and other wirings with large forces. Therefore, these robots are difficult to apply to long-distance, narrow pipe inspections. The cilia vibration type and the spirochete type have relatively compact mechanisms. Nevertheless, these robots are difficult to apply to long-distance inspections because of the low traction due to their structure. The earthworm type is often driven by fluid pressure. They are composed of multiple connected segments. These segments' radial expansion and axial contraction are transmitted from the front to the back to propagate while gripping the pipe. The large axial contraction due to fluid pressure provides large traction even with a small mechanism. However, the propulsion depends on the passive elasticity of the segment's material. The material becomes rigid to obtain large propulsion and the robot lacks flexibility.

In contrast, the inchworm type has connected gripping parts and extension parts. The gripping parts hold the robot inside the pipe, while the extension parts extend the robot to move the robot forward. The large extension force from the fluid pressure provides a large propulsion even with a compact structure. Nevertheless, traction depends on passive elasticity. Therefore, the large passive elasticity reduces flexibility. Thus, developing a compact, flexible robot that can enhance both traction and propulsion has been difficult. So, there is a need to develop a compact robot to amplify both traction and propulsion with flexibility.

This study aims to develop a flexible in-Pipe Inspection Robot capable of enhancing traction and propulsion using a large force generated by hydrodynamic actuators. The goal is to achieve long-distance, small-diameter, complex pipe inspection with the in-Pipe Inspection Robot. Thus, we considered the force generation principles using a fluid pressure-driven actuator in a narrow pipe. The force generated by fluid pressure was determined by multiplying the cross- sectional area by the pressure. The integrated force was not increased because the actuators in parallel had a divided cross- sectional area in the pipe. Therefore, considering the principle of fluid pressure force, a system with large traction and propulsion by serially concatenated actuators in a long, narrow pipe was needed. Therefore, we proposed the linear antagonistic mechanism. The mechanism consisted of a gripping actuator to fix the robot sandwiched by two extension actuators. The distance between the two end faces of the two extension actuators was constrained not to change. When one of the extension actuators was actively extended while the central gripping actuator was fixed in the pipe, the other extension actuator was forced to contract. Thus, the mechanism could exert both traction and propulsions through the active extension fluid pressure force.

In a previous study [29], [30], we developed an in-Pipe Inspection Robot PI-RO and PI-RO II (Pipe Inspection Robot) having a linear antagonistic mechanism. The PI-RO had 2.57 times higher Dimensionless evaluation function for the sum of the traction and propulsion force than the other works considering differences in applied pressure and pipe inner diameter [29]. Furthermore, the PI-RO was achieved to move in the pipe with an inner diameter of 28 mm, a length of 11.7 m, and a bend. However, PI-RO had less traction when exerting a large propulsion to pass through a bending pipe. This is because the linear antagonistic mechanism distributed the force with one actuator into the traction and propulsion. Therefore, PI-RO II was devised to enhance the traction, and initial studies were conducted [30]. However, the robot in the previous study could not pass through the curved pipe because the travel path of PI-RO II changed in the bends, and the actuator's displacement was not efficiently converted into PI-RO II's displacement. Particularly, when passing through a series of bends over a short distance, a large displacement is required, therefore, PI-RO II's traction was lacking at a series of bends of long pipes. Moreover, PI-RO II with the enhanced linear antagonistic mechanism and other robots was not quantitatively compared, hence, the effectiveness of the mechanism was not demonstrated.

This paper describes an enhanced linear antagonistic mechanism increasing traction with high propulsion and flexibility considering pipe radius of curvature, as shown in Fig. 1. Therefore, PI-RO II incorporating this mechanism was developed to inspect pipes similar to a factory pipe, with a maximum length of 20 m, an inner diameter of 35.5 mm, stainless steel material of, and up to 8 bends. Assembling the robot within the limited space of a pipe to increase the traction by simply increasing the number of actuators in a linear antagonistic mechanism was difficult. This is due to the increase in wiring to drive the actuators. Therefore, we increased the traction without significantly increasing the number of actuators. Specifically, the actuators used in the linear antagonistic mechanism were regarded as variable stiffness springs, and the spring constant was increased by synthesizing. Moreover, the diameter of the extension unit was designed to reduce the loss caused by force for Yaw and Pitch directions in a bend from PI-RO II's path change model.

In section II, the design method of PI-RO II is described, and in section III, the configuration of PI-RO II and its basic characteristics related to traction and propulsion are described. Section V discusses the results of the comparison of the traction and propulsion and flexibility of the PI-RO II based on the evaluation function. Finally, section VI describes the summary and future work. The contributions of this paper are listed below.

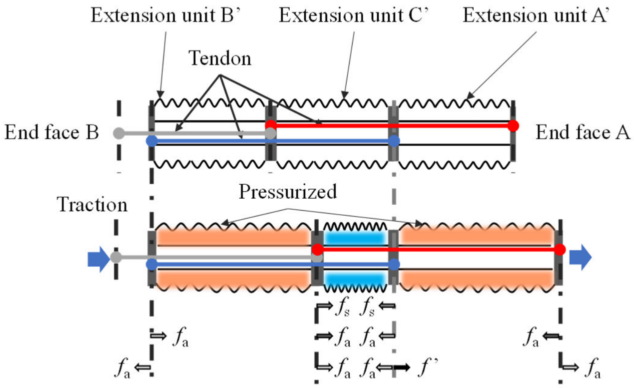

FIGURE 1. The concept of the enhanced linear antagonistic mechanism.

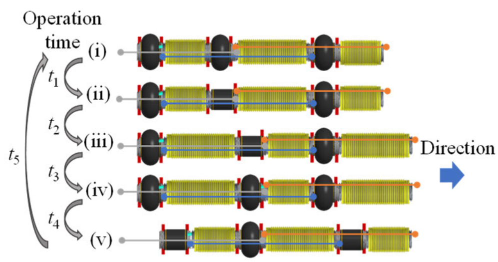

FIGURE 2. Operation pattern of pipe inspection robot (PI-RO) II moving in ① to ⑥.

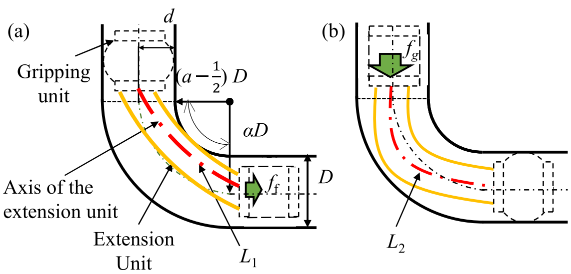

FIGURE 3. A path model of pipe inspection robot (PI-RO) II in passing through an elbow pipe. (a) The travel path of (iii), as shown in Fig. 2. (b) The travel path of (iv), as shown in Fig. 2.

- A model for PI-RO II with a mechanism to pass through a bend was developed, and its performance was demonstrated by experiments.

- The robot with the enhanced linear antagonistic mechanism to enhance traction was developed and the traction and propulsion were measured.

- The quantitative comparison was made with the other in-pipe robots based on the dimensionless index regarding the pipe's inner diameter and applied pressure.

II. DESIGN

This section describes the enhanced linear antagonistic mechanism concept, a design method, a model of PI-RO II's path in the bending pipe, and the design of the extension and gripping units and configuration of PI-RO II to reduce changes in the travel path.

A. LINEAR ANTAGONISTIC MECHANISM AND ITS CHALLENGES

A previous study proposed a linear antagonistic mechanism composed of an actuator that fixed the mechanism location connected to two extension units [29]. This paper presents the mechanism with enhanced pulling force to increase the traction of the in-Pipe Inspection Robot.

The extension units had nonlinear spring characteristics in the axial direction when the applied pressure was constant [29]. Increasing the synthesized spring constants of multiple extension units led to an increase in pulling force. Table 1 shows the parameters used in the synthesis, and Table 2 shows the method of synthesizing spring constants and spring constants. The synthesized spring constants increased above the average of k_1 and k_2 in I. and III. and decreased in II.I. did not increase the spring constant in the narrow pipe due to the division of the cross- sectional area. Therefore, we proposed an enhanced linear antagonistic mechanism based on the synthesis method of III. to increase the traction.

B. ENHANCED LINEAR ANTAGONISTIC MECHANISM

An enhanced linear antagonistic mechanism operation is shown in Fig. 1. This mechanism consisted of three extension units A', B', C', and three tendons. Also, the linkage parts of each unit were actively fixed and released. When the right-side linkage parts were fixed, the active push-in force acted on end-face A from the active pushing force of extension unit A', and the pushing force was transmitted to end-face B by the tendon connected to end-face A. Simultaneously, the active pushing force of the extension unit B' and the passive contracting force of the extension unit C' were transmitted to the end-face B.

Fig. 2 shows the propulsion F_{Pro} and the traction F_{Tra} generated by the mechanism in Eqs. (1) and (2) using the definitions in Table 1. From Eq. (1), the force acting on the end-face B, which is converted traction F_{Tra}, is $(2f_{\mathrm{a}} + f_{\mathrm{s}})/(f_{\mathrm{a}} + f_{\mathrm{s}})$ times larger than that of the linear antagonistic mechanism [29]. When f_{a} is sufficiently large relative to f_{s}, F_{Tra} is twice.

$$F_{\mathrm{Pro}} = f_{\mathrm{a}} \tag{1}$$
$$F_{\mathrm{Tra}} = 2f_{\mathrm{a}} + f_{\mathrm{s}} \tag{2}$$

C. CONFIGURATION AND MOVEMENT PATTERNS OF PI-RO II

Fig. 2 shows the operation pattern configuration of PI-RO II. PI-RO II consisted of three gripping units and three extension units. In a preliminary experiment, when a force in the Yaw and Pitch direction from a pulling object acted on the rearmost PI-RO II, the rearmost extension unit bent, and the extension force was difficult to be transmitted. Therefore, the gripping unit was connected at the rearmost part to keep the extension unit's axis parallel with the pipe axis to efficiently convert the extension unit's force as traction.

The operation of PI-RO II is described below. (i) The three gripping units griped a pipe while the central extending unit

TABLE 1. List of symbols and nomenclatures of the linear antagonistic mechanisms and spring constant.

Symbol	Definition	Unit
f_a	Active extension force of the extension unit	N
fs	Passive contraction of the extension unit	N
f'	Force in the axial direction of the fixed end	N
F_{Pro}	Propulsion by the mechanism	N
F_{Tra}	Traction by the mechanism	N
k_1, k_2	The spring constant	N/mm
k_I, k_{II}, k_{III}	The composite spring constant of each method	N/mm

TABLE 2. The composite spring constant and the calculation.

Combined spring rate		Combined method
I.	$k_I = k_1 + k_2$	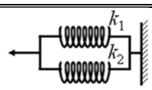 Parallel
II.	$k_{II} = \frac{k1 \cdot k2}{k1 + k2}$	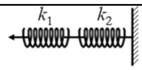 Serial
III.	$k_{III} = k_1 + k_2$	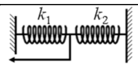 Sandwich

was extended. (ii) The central gripping unit released the pipe. (iii) The extension units at both ends were extended and the tendon mechanism exerted the force shown in Eq. (2) in the right direction. (iv) The central gripping unit gripped the pipe. (v) The front and rear gripping units released the pipe. (vi) The central extension unit was extended and the extension units at both ends were contracted. PI-RO II moved forward by repeating the movements from (i) to (vi).

A camera is installed at the front of the PI-Ro II (tip of the robot, on the right side of the paper) to capture images of the inside of the pipe. When moving forward deep into a pipe, the robot requires a large tractive force. By contrast, the robot can generate a force when moving backward by pulling on the wiring that is pulled by PI- RO II. Therefore, the robot can use the wiring as a guide to move backward even if the backward-facing camera image of the robot is not visible.

D. THE PATH MODEL IN BENDING PIPES

This section describes a travel path change model of PI-RO II due to forces in the Yaw and Pitch directions when passing through a bending pipe. The extension unit in the middle of PI-RO II pulled the wiring at (iii), as shown in Fig. 2, and pushed PI-RO II at (iv). Fig. 3(a) and Fig. 3(b) show the states of (iii) and (iv), respectively when PI-RO II was subjected to loads from the tractive and propulsive directions during passing through a bending pipe.

Due to the tension f_f acting on the towed wirings, PI-RO II's path is L_1 when (iii). By contrast, PI-RO II passes through the path L_2 due to f_g from the front when (iv). Defining $L_p = L_2$- L_1 and l_e as the elongation distance of the extension unit, respectively, PI-RO II theoretically passes through the bending pipe without stopping when $l_e > L_p$. If PI-RO II passes through the shortest path when (iii) and the longest path when (iv), L_p is expressed by Eq. (3). Therefore, we designed the extension unit to reduce L_p. Then, l_e was designed to be larger than L_p.

$$L_p = \theta (D - d) \tag{3}$$

E. GRIPPING UNIT

Fig. 4(a) shows the prototype gripping unit's appearance. The unit used a straight-fiver-type artificial muscle [31]. When air pressure was applied, the unit expanded in the radial direction, beyond the pipe's inner diameter and gripping. When the applied air was exhausted, the unit returned to its initial state due to the elasticity of the constituent materials and stopped gripping. The unit was surrounded by a nylon brush [32], reducing the frictional force caused by the gripping unit contacting the pipe's inner wall. Table 3 shows the specifications of the artificial muscle.

Fig. 4(b) and Fig. 4(c) show the internal pressure and contraction response of the gripping unit, respectively. Air pressure controlled by the proportional solenoid valve ITV2050 was applied to the gripping unit through an air tube with an inner diameter of 1 mm and length of 0.8 m, which was connected to an air tube with an inner diameter of 2.5 mm and a length of 20 m via a rapid exhaust valve, as in a previous study [29]. Fig. 4(b) shows that when 0.25 MPa was applied, the internal pressure reached 95% of the pressure at 1.7 s. In contrast, when 0.25 MPa was applied, as shown in Fig. 4(c), the maximum contraction amount occurred at 1.8 s. Thus, when 0.25 MPa was applied to the gripping unit as the upstream pressure for 1.8 s or longer, the internal pressure increased more than 0.95 times while the gripping unit gripped the pipe. The maximum contraction of the gripping unit was 17 mm, which is almost constant at pressures higher than 0.20 MPa, as shown in Fig. 4(c).

Fig. 4(d) shows the maximum static friction force of the gripping unit. The maximum static friction force increased linearly with the internal pressure. We considered that the artificial muscle force pressing against the pipe increased with the increase in pressure. The maximum static friction force was 368.1 N at a pressure of 0.30 MPa. When the applied pressure was 0.05 MPa, the gripping unit did not expand more than the pipe's inner diameter.

F. EXTENSION UNIT

Fig. 4(e) shows the extension unit. When air pressure was applied, the unit extended in the axial direction, pushing PI-RO II forward. When the applied air was exhausted, the unit returned to its natural length due to the elasticity of the constituent materials. Like the gripping unit, this unit had a hollow structure. From the previous study [29], the theoretical pushing force F_{th} of the extension unit is Eq. (4). Note that the letters and values in Table 4 are adapted in this model. The theoretical pushing force F_{th0} at natural

TABLE 3. Specifications of straight fiber type artificial muscle of the grip unit.

Straight fiber type artificial muscle	
Length [mm]	60
Outer diameter [mm]	18
Thickness [mm]	1
Rubber material	NR
Fiber material	Aramid fiber

TABLE 4. List of symbols and values for the pushing force model.

symbol	Definition	value	Unit
d_e	Outer diameter pressurized cross-section	28	mm
d_e'	Inner diameter pressurized cross-section.	14	mm
P	Applied pressure	-	MPa
k_e	The spring constant of the extension spring	290	N/m
k_r	The spring constant of the rubber tube	119	N/m
k_b	The spring constant of the bellow	43	N/m
F_I	Initial tension of the extension unit	3.84	N
x	Displacement of the extension unit	-	mm
F_{th}	Theoretical pushing force of the extension unit	-	N
F_{th0}	Theoretical pushing force of the extension unit when natural length	-	N

length is given by Eq. (5), and it is the maximum pushing force. Referring to Eqs. (4) and (5), the outer diameter of the pressure-receiving cross-section was designed to be large to gain a large force. When the outer diameter was increased, the travel path change decreased according to Eq. (2). Therefore, the outer diameter of the pressure-receiving cross-section, d_e, is 28 mm, approximately 80% of the pipe's inner diameter. d_e' was 14 mm, allowing wiring to pass through the extension unit designed to be large to gain a large force. When the outer diameter was increased, the travel path change decreased according to Eq. (2). Therefore, the outer diameter of the pressure-receiving cross-section, d_e, is 28 mm, approximately 80% of the pipe's inner diameter. d_e' was 14 mm, allowing wiring to pass through the extension unit.

Fig. 4(f) and Fig. 4(g) is the internal pressure and contraction response of the extension unit, respectively. Air pressure is applied by the same method as the extension unit. Fig. 4(f) shows that when 0.25 MPa was applied, the internal pressure reached 95% of the pressure at 2.6 s. In contrast, when 0.25 MPa was applied, as shown in Fig. 4(g), the maximum contraction amount occurred at 1.8 s. Thus, when 0.25 MPa was applied to the extension unit as the upstream pressure for 2.6 s or longer, the internal pressure increased more than 0.95 times while the gripping unit gripped the pipe. The maximum extension of the extension unit was 50 mm, which is almost constant at pressures higher than 0.15 MPa, as shown in Fig. 4(g).

Fig. 4(h) shows the maximum extension force of the extension unit. The force increased linearly with increasing applied pressure. When 0.25 MPa was applied, the extension force was 123.2 N, which is almost consistent with Eq (5). The measured values exceeded the theoretical values in some conditions. As the outer diameter of the developed extension unit was slightly expanded, we could consider that increased applied air pressure caused the outer diameter d_e of the extension unit to increase and the inner diameter d_e' to decrease, thus increasing the pressure-receiving area of the air pressure. Hence, the measured value was considered to exceed the theoretical value when high pressure was applied. The operation pattern of the PI-RO II was decided considering the characteristics of these units, as shown in Table 5.

$$F_{th} = \frac{\pi P\left(d_e^2 - d_e'^2\right)}{4} - (k_e + k_r + k_b)\,x - F_I \tag{4}$$

$$F_{th0} = \frac{\pi P\left(d_e^2 - d_e'^2\right)}{4} - F_I \tag{5}$$

G. ESTIMATED TRACTION AND TRAVEL PATH CONDITION

The traction was exerted during the transition from (ii) to (iii) in Fig. 2. The steady state is shown in Fig. 5. Each parameter is shown in Table 1, where F is the tension force acting on the pulled object. Fig. 5 shows that PI-RO II was presumed to move without slipping in $F < (2f_a + f_s)$ and the gripping force $f' > (2f_a + f_s)$. The maximum L_p was 19.3 mm when the outer diameter of the extension unit was substituted into the model of a path in a bending pipe. Therefore, the maximum extension length of the extension unit was 50 mm, meaning that PI-RO II could be expected to pass through bending pipes by using the developed extension unit.

III. DEVELOPMENT

This section describes the configuration and basic characteristics of PI-RO II.

A. PI-RO II WITH AN ENHANCED LINEAR ANTAGONISTIC MECHANISM

Fig. 6 is PI-RO II with an enhanced linear antagonistic mechanism. PI-RO II consisted of a head attached to an endoscope, three extension units, three gripping units, and five spring joints connecting these units: pneumatic tubes for driving these units, tendon wires, and a wire for the endoscope for visibility inspecting the pipe through PI-RO.

The joints connecting each unit of the robot are tension springs. As in the previous study [29], the tension spring bends flexibly in the bend pipe and stiffens when transmitting force in the compressive direction to transmit force, thus converting the actuator force utilized in PI-Ro II into traction and propulsion force.

Next, the control method of the PI-Ro II is described. The PI-RO II can move forward and backward by peristaltic motion. The actuator force of the PI-RO II is not accurate as a feature of flexible rubber actuators. However, it can propel itself through bent pipes along the pipe path because the PI-RO II is flexible.

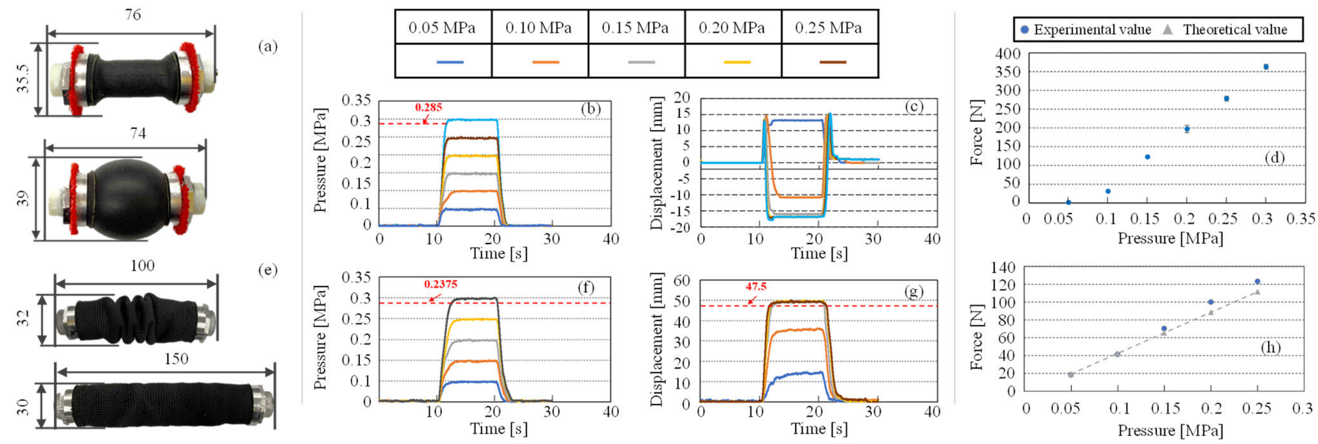

FIGURE 4. Appearance and Characteristics of Actuators Comprising Pipe Inspection Robot (PI-RO) II. (a) The gripping unit. (b) Pressure response of the gripping unit. (c) Displacement response of the gripping unit. (d) Contraction of the gripping unit. (e) The extension unit. (f) Pressure response of the extension unit. (g) Displacement response of the extension unit. (h) Extension force of the gripping unit.

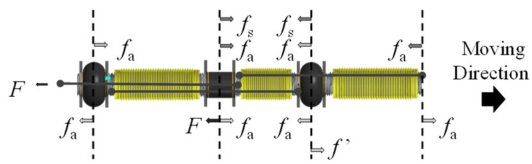

FIGURE 5. The traction model of pipe inspection robot (PI-RO) II.

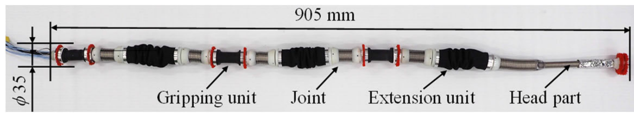

FIGURE 6. Pipe Inspection Robot (PI-RO) II developed in this study.

TABLE 5. Specifications of the straight fiber type artificial muscle of the grip unit.

t_1	t_2	t_3	t_4	t_5
2.5	3.0	2.0	3.0	2.0

B. CHARACTERISTICS OF ROBOT

This section describes the purpose, environment, methods, results, and discussion of traction and propulsion.

1) PURPOSE

The traction and propulsion of the PI-RO II with the proposed enhanced linear antagonistic mechanism are measured. The validity of the proposed model is verified through comparison with the pneumatic characteristics of the extension force of the extension unit and PI-RO with the linear antagonistic mechanism, which the non-enhanced.

2) ENVIRONMENT AND METHOD

The traction and propulsion are measured in the same way as in a previous study [29] as shown in Fig. 7. In the propulsion measurement, PI-RO II is placed in a stainless-steel pipe with a load cell on one side as shown in Fig. 7 (a). Then, PI-RO II moves toward the direction of compression of the load cell for 150 s in the pipe, and the force is measured as the propulsion. The load cell and PI-RO II are connected using a wire, and the PI-RO II is moved in the opposite direction in which the load cell is installed in the pipe for 150 s. The load cell connected by the wire is pulled, and the tension force was measured as the traction as shown in Fig. 7 (b). The sampling frequency is 2 kHz, and 0.30 MPa is applied to the gripping unit. The extension unit is applied at 0.05 - 0.25 MPa at 0.05 MPa increments. The operation times shown in Table 5 are applied to the PI-RO II.

3) RESULTS

Fig. 8(a) and (b) shows that traction and propulsion at 0.2 MPa were applied to the extension unit as a representative sample. Fig. 8(c) and (d) shows the time series data of traction and propulsion. Fig. 8(f) shows the relationship between the maximum traction and the applied pressure.

4) DISCUSSION

Fig. 8 (a), (b), (c), and (d) shows that the traction and propulsion started to increase from the operation beginning and reached a steady state. These forces increased while vibrating until the play was removed. The force waveform then follows a constant period while vibrating. The vibrations indicate that PI-Ro II is periodically propelled, as shown in Fig. 2, and that traction and propulsion are periodically exerted. After a certain duration, the extension unit was almost no longer extended, then the traction and propulsion were in constant vibration. In-pipe robots driven by air pressure, like PI-RO II, repeated a constant motion. Hence, we considered that the force peaks were inflated, when the units at both ends extend and decreased when the gripping units at both ends were exhausted. The traction and propulsion increased as the applied pressure increased. Both traction and propulsion increase linearly in force with respect to air pressure.

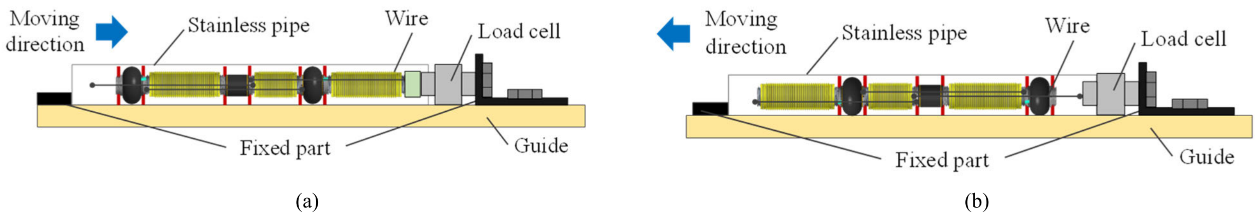

FIGURE 7. Force measuring setup. (a) Experimental environment for measuring propulsion force. (b) Experimental environment for measuring traction force.

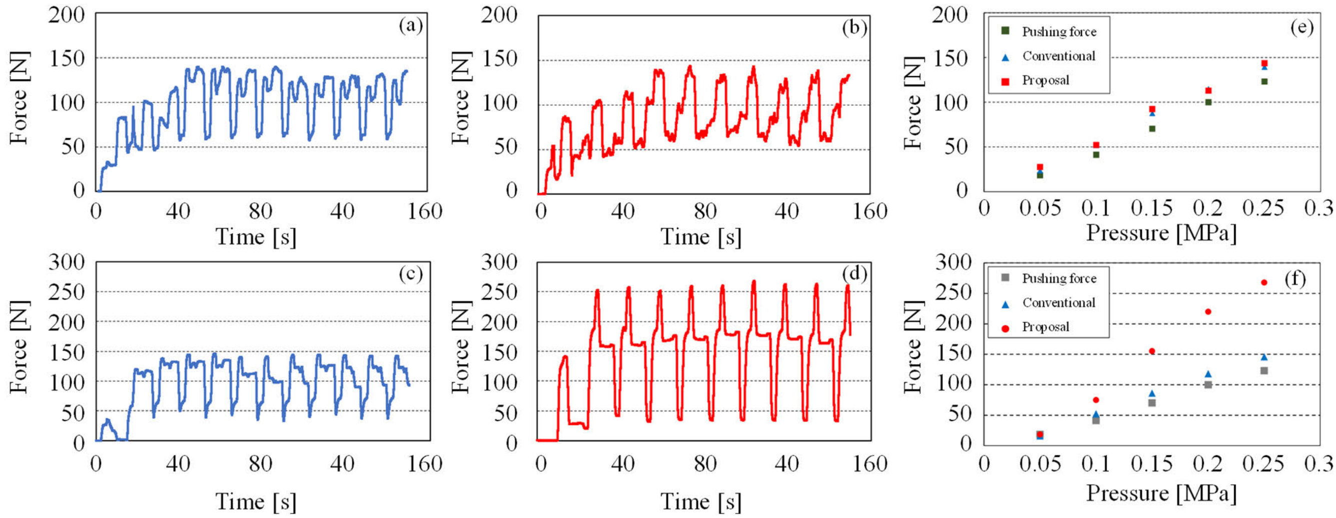

FIGURE 8. Time series Pipe Inspection Robot (PI-RO)'s traction and propulsion and comparison of their maximum values. The traction and propulsion data at 250 kPa applied to PI-RO with the linear antagonistic mechanism and PI-RO II with the enhanced linear antagonistic mechanism are described. (a) Propulsion (a linear antagonistic mechanism). (b) Traction (a linear antagonistic mechanism). (c) Propulsion (an enhanced linear antagonistic mechanism). (d) Traction (an enhanced linear antagonistic mechanism). (e) Comparison of the propulsion and the force generated by the extension unit. (f) Comparison of traction and the force generated by the extension unit.

These results are similar to those obtained for the pressure characteristics of the actuator. Therefore, we considered that traction and propulsion could be generated actively. However, there was a difference between the propulsion and the push-in force of the extension unit. In the experiment, the extension unit received a compressive force, which changed the outer diameter of the unit and increased the pressure-receiving area. We considered that compression force indirectly increased propulsion.

Fig. 8(f) shows that when 0.25 MPa was applied to the extension unit, the maximum traction was 146.1 N for the PI-RO with linear antagonistic mechanism and 1.84 times the maximum traction of 268.1 N for PI-RO II with the enhanced linear antagonistic mechanism. The maximum theoretical traction was 145.1 N for PI-RO and 1.85 times the maximum theoretical traction of 268.3 N for PI-RO II. Therefore, the theoretical and measured values were close to each other. Therefore, we believe that the proposed model is valid, and the traction of the robot increased using the proposal mechanism.

IV. EXPERIMENT

This section describes the passage performance test results of PI-RO II with the enhanced linear antagonistic mechanism. The test course was largely divided into two parts: A. Basic pipe passage and B. Passage in pipeline simulated in the factory, including a series of bending pipes over a short distance, which failed to pass through PI-RO with the linear antagonistic mechanism in the preliminary experiment.

A. BASIC PIPE PASSAGE (HORIZONTAL AND VERTICAL, ELBOW)

This subsection describes the passage performance of PI-RO II in the pipe constituting the pipeline simulated in the factory.

1) PURPOSE

The moving performance of PI-RO II was verified in the horizontal and vertical straight pipes and elbow pipes.

2) ENVIRONMENT AND METHOD

PI-RO II moves in a 2 m straight transparent acrylic pipe installed horizontally and vertically with the ground and in a 1 m pipe with an elbow pipe installed horizontally with the ground. A video camera captures PI-RO II, and the passage time is measured from the video images. The operation times shown in Table 5 were applied to the PI-RO II.

3) RESULTS

The speeds in the horizontal and vertical transparent acrylic pipes were 3.57 mm/s in both cases. In contrast, the traveling speed was 3.34 mm/s for the elbow pipe passage.

4) DISCUSSION

PI-RO II moved the horizontal and vertical pipes at the same speed. Therefore, we believe that the traction and propulsion of PI-RO II exceeded its weight effect. Meanwhile, there was a decrease in the speed during the elbow pipe passage. Inside the elbow pipe, the extension unit bent, and the extension amount decreased. Therefore, the speed at which the elbow pipe passed through the elbow pipe was thought to have increased.

B. BASIC PIPE PASSAGE (HORIZONTAL AND VERTICAL, ELBOW)

This subsection describes the passage performance of PI-RO II in the pipeline simulated in the factory, including a series of bending pipes over a short distance.

1) PURPOSE

The passage performance of PI-RO II is verified in the pipeline simulated in the factory, including a series of bending pipes over a short distance.

2) ENVIRONMENT AND METHOD

Fig. 9 shows the simulated pipeline. The layout is simulated as an actual factory piping layout. There are 5 elbow pipes with a length of 4.5 m pipeline. The passage performance of the PI-RO II is tested in the pipe from point A to point B three times. The experiment is started by placing the head of PI-RO II at a point 1 m into the pipe from point A. The operation times shown in Table 5 were applied to the PI-RO II.

3) RESULTS AND DISCUSSION

The test results are shown in Fig. 10. PI-RO II consecutively passed through the pipeline simulated in the factory three times. The duration of the three tests was approximately 1250 s.

RI-Ro II passed through the pipes that PI-RO could not pass through. Therefore, we believe that the proposed mechanism is effective. The average speed of PI-RO II was 2.81 mm/s (3.62 mm/s per pipe length), almost the same in all three tests, indicating a high reproducibility of this experiment. Compared to the horizontal pipe, the moving speed was 0.79 times slower. When PI-RO II propelled through the piping, the frictional force and gravity acting on the wiring increased. Therefore, we believe these forces reduced the speed of PI-RO II. However, PI-RO II enabled passage in the pipeline simulated in the factory, including a series of bending pipes over a short distance. Thus, we expect the enhanced linear antagonistic mechanism can realize the inspection of long, narrow, and complex pipes.

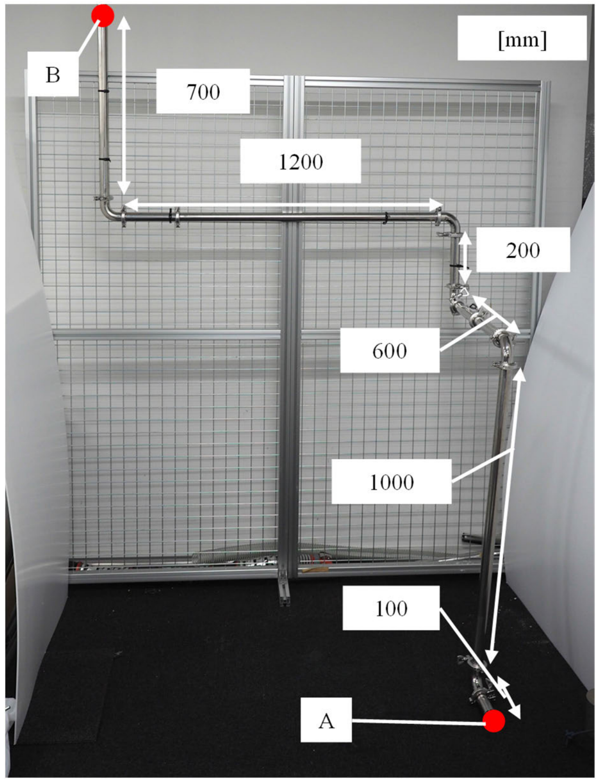

FIGURE 9. The pipeline simulated in the factory with a series of bending pipes over a short distance, which failed to pass through the pipe inspection robot (PI-RO) with the linear antagonistic mechanism in the previous experiment. The inspection tests were performed by a robot from A to B.

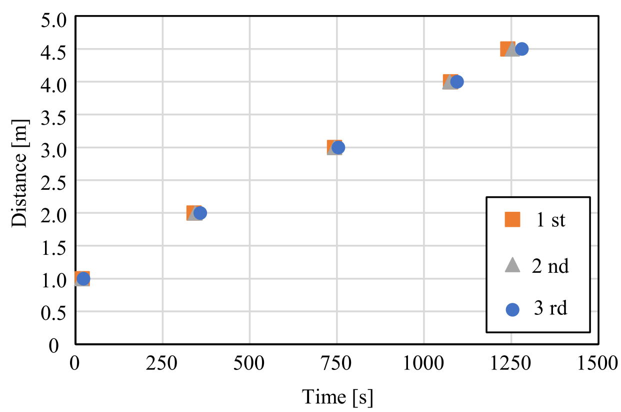

FIGURE 10. Results of the passage test in pipelines simulated in the factory.

V. SUMMARY AND DISCUSSION OF PI-RO II

The enhanced linear antagonistic mechanism enhanced traction. The designed extension units efficiently converted the extension force into traction, enabling PI-RO II to pass through the pipeline that failed to pass through PI-RO with the linear antagonistic mechanism.

In this section, we present a numerical comparison of the traction and propulsion of PI-RO II with robots operating on similar principles. We evaluated the traction and propulsion based on the evaluation function of a previous

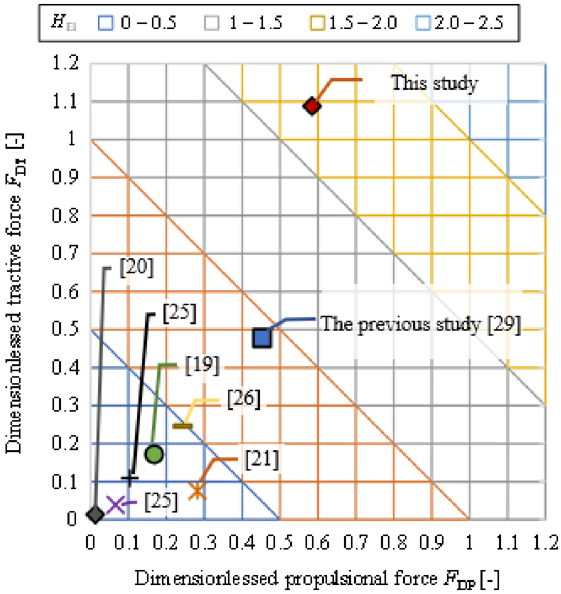

FIGURE 11. Comparison of evaluation functions. Pipe Inspection Robot (PI-RO) II had a 1.79 times higher HEI value than PI-RO in the previous study [29].

study [29]. This evaluation function is dimensionless and comparable to the mechanically available forces, even when the scale and applied pressure of the robot are different. Generally, the traction increases as the inspection distance increases. Conversely, the propulsion depends on the shape of the pipe to be inspected regardless of the inspection distance. Therefore, the balance between the traction and propulsion of the robot was also evaluated. The evaluation function is shown in Eqs. (6), (7), and (8). Eqs. (6) and (7) show the non-dimensionalized traction F_{DP} and the non-dimensionalized propulsion F_{DT}, respectability. Eq. (8) is the sum of Eqs. (6) and (7) representing the evaluation function H_{EI} in the previous study.

The H_{EI} values are shown in Fig. 11, showing that PI-RO II had 1.79 times higher than PI-RO in a previous study [29]. Compared to PI-RO, the $F_{DT,}$ and F_{DP} of PI-RO II were 2.28 and 1.28 times higher, respectively. Based on the results above, we can expect the enhanced linear antagonistic mechanism to enable the in-pipe robot to perform long-distance inspections, as the traction was significantly increased. Although the propulsion was almost the same as that of the previous study, the PI-RO II could pass through complex pipes, as shown in Fig. 9. Thus, it is expected that the PI-RO II, which was developed by generating both traction and propulsion as active generation force by air pressure, will enable inspection in long, narrow, and complex pipes.

$$F_{DT} = \frac{F_{Tra}}{A \cdot P} \tag{6}$$

$$F_{DP} = \frac{F_{Pro}}{A \cdot P} \tag{7}$$

$$H_{EI} = F_{DP} + F_{DT} \tag{8}$$

VI. CONCLUSION

This paper proposed an enhanced linear antagonistic mechanism increasing traction with high propulsion and flexibility. Moreover, the design of the extension unit reducing the loss by force for Yaw and Pitch directions from a bending pipe from PI-RO II's path change model was described.

From the results, PI-RO II developed in this study exerted maximum propulsion of 146.1 N and maximum traction of 268.1 N. The evaluation function value considering the effects of the applied pressure and the inner diameter of the target pipe of PI-RO II developed in this study was more than 1.79 times compared with other related studies. Furthermore, PI-RO II passed a 4.5 m long complex narrow pipe containing two consecutive curved pipes three times consecutively within 1250 s. These results indicate that the proposed mechanism can realize inspection in complex and narrow pipes over long distances.

The study showed that the developed robot exhibited significant traction and propulsion, which are important for long-distance inspections. However, this paper simulated a sample of pipes installed in a factory due to the ceiling height of the laboratory. In the future, we will verify the long-distance inspection performance of PI-RO II by simulating other piping shapes in a factory.

REFERENCES

[1] D. Mishra, K. K. Agrawal, A. Abbas, R. Srivastava, and R. S. Yadav, "PIG [pipe inspection gauge]: An artificial dustman for cross country pipelines," *Proc. Comput. Sci.*, vol. 152, pp. 333–340, Jan. 2019.

[2] S. Yoda, Y. Wakibe, and Y. Imagawa, "Inspection methods of piping," (in Japanease), *Bull. Soc. Sea Water Sci.*, vol. 68, no. 2, pp. 57–62, Sep. 2014.

[3] A. H. Heidari, M. Mehrandezh, R. Paranjape, and H. Najjaran, "Dynamic analysis and human analogous control of a pipe crawling robot," in *Proc. IEEE/RSJ Int. Conf. Intell. Robots Syst.*, St. Louis, MO, USA, Oct. 2009, pp. 733–740.

[4] H. M. Kim, Y. S. Choi, Y. G. Lee, and H. R. Choi, "Novel mechanism for in-pipe robot based on a multiaxial differential gear mechanism," *IEEE/ASME Trans. Mechatronics*, vol. 22, no. 1, pp. 227–235, Feb. 2017.

[5] J.-H. Kim, G. Sharma, and S. Sitharama Iyengar, "FAMPER: A fully autonomous mobile robot for pipeline exploration," in *Proc. IEEE Int. Conf. Ind. Technol.*, Mar. 2010, Viña del Mar, Chile, pp. 517–523.

[6] A. Kakogawa, Y. Oka, and S. Ma, "Multi-link articulated wheeled in-pipe robot with underactuated twisting joints," in *Proc. IEEE Int. Conf. Mechatronics Autom. (ICMA)*, Changchun, China, Aug. 2018, pp. 942–947.

[7] S.-G. Roh and H. R. Choi, "Differential-drive in-pipe robot for moving inside urban gas pipelines," *IEEE Trans. Robot.*, vol. 21, no. 1, pp. 1–17, Feb. 2005.

[8] H. Shin, K. Jeong, and J. Kwon, "Development of a snake robot moving in a small diameter pipe," in *Proc. IEEE Int. Conf. Control, Autom. Syst. (ICCAS)*, Gyeonggi-do, South Korea, Oct. 2010, pp. 1826–1829.

[9] S. A. Fjerdingen, P. Liljebäck, and A. A. Transeth, "A snake-like robot for internal inspection of complex pipe structures (PIKo)," in *Proc. IEEE/RSJ Int. Conf. Intell. Robots Syst.*, St. Louis, MO, USA, Oct. 2009, pp. 5665–5671.

[10] S. Xiao, Z. Bing, K. Huang, and Y. Huang, "Snake-like robot climbs inside different pipes," in *Proc. IEEE Int. Conf. Robot. Biomimetics (ROBIO)*, Macao, China, Dec. 2017, pp. 1232–1239.

[11] A. Kuwada, K. Tsujino, K. Suzumori, and T. Kanda, "Intelligent actuators realizing snake-like small robot for pipe inspection," in *Proc. IEEE Int. Symp. Micro Nano Mech. Hum. Sci.*, Nagoya, Japan, Nov. 2006, pp. 1–6.

[12] D.-H. Lee, H. Moon, and H. R. Choi, "Autonomous navigation of in-pipe working robot in unknown pipeline environment," in *Proc. IEEE Int. Conf. Robot. Autom.*, Shanghai, China, May 2011, pp. 1559–1564.

[13] M. Konyo, K. Isaki, K. Hatazaki, S. Tadokoro, and F. Takemura, "Ciliary vibration drive mechanism for active scope cameras," *J. Robot. Mechatronics*, vol. 20, no. 3, pp. 490–499, Jun. 2008.
[14] H. Takeshima and T. Takayama, "Development of a steerable in-pipe locomotive device with six braided tubes," *ROBOMECH J.*, vol. 5, no. 1, Dec. 2018, Art. no. 31.
[15] T. Takayama, H. Takeshima, T. Hori, and T. Omata, "A twisted bundled tube locomotive device proposed for in-pipe mobile robot," *IEEE/ASME Trans. Mechatronics*, vol. 20, no. 6, pp. 2915–2923, Dec. 2015.
[16] Y. Mano, R. Ishikawa, Y. Yamada, and T. Nakamura, "Development of high-speed type peristaltic crawling robot for long-distance and complex-line sewer pipe inspection," in *Proc. IEEE/RSJ Int. Conf. Intell. Robots Syst. (IROS)*, Madrid, Spain, Oct. 2018, pp. 8177–8183.
[17] M. Takahashi, I. Hayashi, N. Iwatsuki, K. Suzumori, and N. Ohki, "The development of an in-pipe microrobot applying the motion of an earthworm," in *Proc. 5th Int. Symp. Micro Mechatronics Hum. Sci.*, Nagoya, Japan, Oct. 1994, pp. 35–40.
[18] H. Tsukagoshi, K. Terashima, and Y. Takai, "A self-propelled catheter capable of generating travelling waves with steering function by mono-line drive," in *Proc. IEEE Int. Conf. Robot. Autom. (ICRA)*, Brisbane, QLD, Australia, May 2018, pp. 38–43.
[19] K. Nomura, M. Sato, H. Takeuchi, K. Minoru, T. Ryoichi, H. Ishii, and A. Takanishi, "Development of in-pipe robot with extension hose and balloons," in *Proc. IEEE Int. Conf. Mechatronics Autom. (ICMA)*, Takamatsu, Japan, Aug. 2017, pp. 1481–1486.
[20] T. Yamamoto, M. Konyo, and S. Tadokoro, "A high-speed locomotion mechanism using pneumatic hollow-shaft actuators for in-pipe robots," in *Proc. IEEE/RSJ Int. Conf. Intell. Robots Syst. (IROS)*, Hamburg, Germany, Sep. 2015, pp. 4724–4730.
[21] J. Qiao, J. Shang, and A. Goldenberg, "Development of inchworm in-pipe robot based on self-locking mechanism," *IEEE/ASME Trans. Mechatronics*, vol. 18, no. 2, pp. 799–806, Apr. 2013.
[22] M. Kamata, S. Yamazaki, Y. Tanise, Y. Yamada, and T. Nakamura, "Morphological change in peristaltic crawling motion of a narrow pipe inspection robot inspired by earthworm's locomotion," *Adv. Robot.*, vol. 32, no. 7, pp. 386–397, Jan. 2018.
[23] L. Wang, T. Akagi, S. Dohta, and T. Kawasaki, "Development of slide type inspection robot using flexible pneumatic cylinder," in *Proc. Int. Conf. Adv. Mech. Syst.*, Tokyo, Japan, Sep. 2012, pp. 75–80.
[24] K. Miyasaka, G. Kawano, and H. Tsukagoshi, "Long-mover: Flexible tube in-pipe inspection robot for long distance and complex piping," in *Proc. IEEE/ASME Int. Conf. Adv. Intell. Mechatronics (AIM)*, Auckland, New Zealand, Jul. 2018, pp. 1075–1080.
[25] H. Heung, P. W. Y. Chiu, and Z. Li, "Design and prototyping of a soft earthworm-like robot targeted for GI tract inspection," in *Proc. IEEE Int. Conf. Robot. Biomimetics (ROBIO)*, Qingdao, China, Dec. 2016, pp. 497–502.
[26] B. Zhang, Y. Fan, P. Yang, T. Cao, and H. Liao, "Worm-like soft robot for complicated tubular environments," *Soft Robot.*, vol. 6, no. 3, pp. 399–413, Jun. 2019.
[27] S. Kodama, Y. Konishi, K. Shindo, S. Senzaki, T. Nakamura, Y. Ohnuki, M. Konno, H. Isii, and A. Takanishi, "Development of pneumatic driven robot system which can entry and retire from gas pipe," in *Proc. IEEE Int. Conf. Mechatronics Autom. (ICMA)*, Takamatsu, Japan, Aug. 2021, pp. 1466–1471.
[28] J. Lim, H. Park, S. Moon, and B. Kim, "Pneumatic robot based on inchworm motion for small diameter pipe inspection," in *Proc. IEEE Int. Conf. Robot. Biomimetics (ROBIO)*, Sanya, China, Dec. 2007, pp. 330–335.
[29] F. Ito, K. Takaya, M. Kamata, M. Okui, Y. Yamada, and T. Nakamura, "In-pipe inspection robot capable of actively exerting propulsive and tractive forces with linear antagonistic mechanism," *IEEE Access*, vol. 9, pp. 131245–131259, 2021.
[30] F. Ito, K. Takaya, H. Sato, J. Watanabe, and T. Nakamura, "Wave propagation type pipe inspection robot with the linear antagonistic mechanism for enhancing traction force—Increasing tractive force with a small number of drive units using superposition of linear antagonistic mechanisms," (in Japanese), *J. Robot. Soc. Jpn.*, vol. 39, no. 7, pp. 665–668, 2021.
[31] T. Nakamura, "Experimental comparisons between McKibben type artificial muscles and straight fibers type artificial muscles," *Proc. SPIE*, vol. 6414, Jan. 2007, Art. no. 641426.
[32] F. Ito, T. Kawaguchi, M. Kamata, Y. Yamada, and T. Nakamura, "Proposal of a peristaltic motion type duct cleaning robot for traveling in a flexible pipe," in *Proc. IEEE/RSJ Int. Conf. Intell. Robots Syst. (IROS)*, Macao, China, Nov. 2019, pp. 6614–6621.

F. ITO (Graduate Student Member, IEEE) received the B.S. and M.S. degrees in engineering from Chuo University, Tokyo, Japan, in 2019 and 2021, respectively, where he is currently pursuing the Ph.D. degree with the Biomechatronics Laboratory.

He has been a JSPS Research Fellow DC1, since 2021. He was a recipient of the IEEE Robotics and Automation Society Japan Joint Chapter Young Award in IEEE/RSJ International Conference on Intelligent Robots and Systems (IROS 2019), in 2019.

Y. NARUSE received the B.S. degree in engineering from Chuo University, Tokyo, Japan, in 2020, where he is currently pursuing the M.S. degree with the Biomechatronics Laboratory.

K. TAKAYA received the B.S. and M.S. degrees in engineering from Chuo University, Tokyo, Japan, in 2019 and 2021, respectively. He has been with Panasonic after getting M.S. degree.

J. WATANABE received the Ph.D. degrees in biological science and in environmental science from the University of Shizuoka, in 2013. In 2014, he joined Pigeon Home Products Corporation, where he has engaged in quality control operations with a manufacturing plant for cosmetics, quasi-drugs, and miscellaneous products.

T. NAKAMURA (Member, IEEE) was born in 1975. He received the B.S. and M.S. degrees in mechanical engineering from Akita University, Akita, Japan, in 1997 and 1999, respectively, and the Ph.D. degree from Shinshu University, Nagano, Japan, in 2003.

From 1999 to 2003, he taught as a Research Associate with Akita Prefecture University, Akita. In 2004, he was a Lecturer with the Faculty of Science and Engineering, Chuo University, Tokyo, Japan. From 2006 to 2013, he was an Associate Professor with Chuo University, where he has been a Professor, since 2013. From 2012 to 2013, he was a Visiting Professor with the Swiss Federal Institute of Technology, EPFL, Lausanne, Switzerland. He is also the current Chairperson of Solaris Inc. His research interests include development and control, such as an artificial muscle, functional fluid, and the development and applications of biorobotics.